J. Coat. Technol. Res., **12** (1) 137–152, 2015
DOI 10.1007/s11998-014-9613-8

Titanium dioxide/conducting polymers composite pigments for corrosion protection of cold rolled steel

Niteen Jadhav, Victoria Gelling

© American Coatings Association 2014

Abstract Titanium dioxide (TiO_2)/conducting polymers composite pigments were synthesized by chemical oxidative polymerization technique in a simple and eco-friendly manner. These composite pigments were characterized for morphology by scanning electron microscopy and transmission electron microscopy, for conductivity by four point probe and conductive-atomic force microscopy, for elemental composition by X-ray photoelectron spectroscopy, and for chemical composition by Fourier transform infrared spectroscopy. Three different types of composite pigments were synthesized, namely TiO_2/polypyrrole composite pigment, TiO_2/polypyrrole composite pigment doped with tungstate anion, and TiO_2/polyaniline composite pigment. Core and shell morphology was obtained for TiO_2/polypyrrole composite pigment and TiO_2/polypyrrole composite pigment doped with tungstate anion. Coatings based on these pigments were formulated and applied on a cold rolled steel substrate. Constant immersion in 5% sodium chloride was employed for studying the corrosion resistance offered by composite pigments-based coatings. The corrosion resistance of the coatings was monitored by electrochemical impedance spectroscopy (EIS) and potentiodynamic polarization technique. EIS results demonstrated increased corrosion protection for the core and shell TiO_2/polypyrrole composite, TiO_2/polypyrrole (tungstate doped) composite, and TiO_2/polyaniline composite. Additionally, potentiodynamic scan results demonstrated passivation achieved by synthesized composite pigments-based coatings, suggesting improved corrosion protection.

N. Jadhav (✉), V. Gelling
Department of Coatings and Polymeric Materials, North Dakota State University, Fargo, ND 58102, USA
e-mail: niteen.jadhav@my.ndsu.edu; n3.uict@gmail.com

Keywords Composite coatings, Corrosion protection, Polypyrrole, Polyaniline, Electrochemical impedance spectroscopy

Introduction

The worldwide yearly corrosion cost is approximately 2.2 trillion USD which amounts to almost 3% of the world's total GDP.[1] Out of total metal under utilization, one-third is often destroyed by corrosion.[2] Corrosion impacts several categories of human civilization, such as infrastructure, transportation, manufacturing, and utilities.[3] Taking into consideration the effects of corrosion on human life and safety, corrosion associated costs, and the need to conserve and prolong the usage of materials, it becomes imperative for researchers to study the details of corrosion and determine the necessary solutions.[4] The process of corrosion transforms metal to its native oxide form mostly by combining with oxygen and water. The metal oxide is metal's natural lowest energy state. Therefore, it is very difficult to stop the corrosion. However, it is possible to mitigate corrosion by using various methods such as coatings, inhibitors, cathodic protection, judicial material selection, and proper design.[5]

The application of protective coatings has been one of the most efficient methods for corrosion protection. One-third of paint produced is applied on metal for its protection and decoration.[6] Protective coatings can be classified as barrier, conversion, anodic, and cathodic coatings. Barrier type coatings are further subdivided into four types: anodic oxides, inhibitive coatings, organic coatings, and inorganic coatings. Barrier type coatings prove ineffective once a defect is formed. Chromates, which are well known and highly effective anti-corrosion agents, are mutagenic and carcinogenic in nature.[7] Metal-rich primers need high pigment volume concentration (PVC) for the necessary electri-

cal contact for corrosion protection. Furthermore, these metals, such as zinc, have a negative environmental impact. Taking into consideration the limitations of existing coating systems, along with the changing environment, rapidly growing heavy industrialization, and increasing pollutants, there is need to find environmentally benign solutions to corrosion with superior properties.

Conducting polymers (CPs) are a relatively new class of materials with interesting properties such as conductivity, good environmental stability, easy supply, and facile synthesis procedures.[8,9] Owing to these properties, CPs find numerous applications, including sensors,[10] actuators,[11] electrochemical devices,[12] electrochromic cells,[13] batteries,[14] solar cells,[15] light emitting devices,[16] drug delivery,[17] and corrosion protection.[18] Mengoli et al.[19] were the first to explore CPs for corrosion inhibition. This was followed by several research articles over the last three decades demonstrating the usefulness of CPs for corrosion inhibition.[20–26] CPs can be synthesized by chemical oxidative polymerization or electrochemical polymerization. Large scale synthesis is possible with chemical oxidative polymerization along with the possibility of covalent modification of the CPs backbone. Several new monomers and modified monomers can be easily polymerized by chemical oxidative polymerization.[27]

Polyaniline (PANI), polypyrrole (PPy), and polythiophene (PTh) are most widely studied CPs for the corrosion inhibition on metal and metal alloys substrates.[28,29] PPy is widely studied for the corrosion protection of metals and metal alloys owing to its properties such as good conductivity, better environmental stability, nontoxicity, thermal stability, and ease of synthesis.[30–32] However, PPy has drawbacks such as insolubility, stiff chains, poor mechanical properties, difficult processibility, irreversible charge consumption in redox process, and porosity.[33–35] In order to overcome these problems associated with the application of PPy, various avenues have been employed by several researchers, including chemical modification of the pyrrole monomer, dopant incorporation, copolymerization, composites and nanocomposites of CPs with inorganic materials, and multilayers of CPs.[36–39]

Incorporation of composites of PPy and inorganic pigments into coatings is a promising method for overcoming drawbacks associated with PPy use in the coatings.[40] Inorganic pigments are widely used in the coatings industry for hiding, color, mechanical strength, chemical resistance, and thermal stability.[41] A combination of these inorganic pigments with PPy could impart the properties of both PPy and the inorganic pigments for a synergistic effect. Composites of PPy and inorganic pigments have been synthesized for corrosion protection of steel by electrochemical methods.[42,43] Titanium dioxide (TiO_2)/PPy composite was electrochemically prepared on AISI 1010 steel and it was found that the incorporation of TiO_2 into the composite matrix at about 6.5% by weight results in little improvement in corrosion resistance.[44] It was also found that TiO_2 did not interfere in the polymerization of pyrrole when electrochemical polymerization was performed on the surface of mild steel.[45] Sn-doped TiO_2 and PPy nanocomposite was prepared by chemical oxidative polymerization of pyrrole. Then, it was incorporated into epoxy polyamide coating at 1% by weight and applied on mild steel.[46] Similarly, Ni-doped TiO_2 and PPy nanocomposite were also synthesized.[47] Both papers reported improvements in corrosion resistance.

Corrosion-inhibiting dopants can be incorporated on the backbone of PPy. Once PPy is reduced, these corrosion inhibiting dopants can combine with the underlying metal to form an insoluble layer improving the corrosion resistance.[48,49] In contact with the underlying metal, oxidation of metal can induce reduction of PPy, resulting in the release of the dopant anion which could further passivate the defect, demonstrating a smart corrosion protection mechanism.[50] Tungstate-doped PPy was electrodeposited on the surface of carbon steel which showed participation of tungstate anion in the passivation mechanism, resulting in improved corrosion protection.[51] Phosphate and tungstate anion-doped PPy was electrodeposited on mild steel surface demonstrating a better corrosion protection offered by the tungstate anion-doped PPy as compared to phosphate anion-doped PPy.[35] Tungstate has shown good corrosion inhibition for steel.[52]

It has been reported that if effective passivation is not achieved in certain conditions, such as in the presence of a large defect, CPs can act as a corrosion mediator thereby promoting corrosion.[53] In order to avoid this problem and the issues mentioned earlier, CPs-containing pigments (CPCP) have been developed.[43,54–56] Aluminum flakes coated with PPy have been found to provide corrosion protection on the surface of aluminum 2024-T3.

In this article, CPs redox activity and dopant release ability is combined and a composite with TiO_2 is synthesized by chemical oxidative polymerization resulting in unique morphology. Three different types of CPCC were synthesized, namely, TiO_2/PPy composite, TiO_2/PPy (tungstate doped) composite, and TiO_2/PANI composite. These composites were characterized for morphology by scanning electron microscopy (SEM) and transmission electron microscopy (TEM), for composition by Fourier transform infrared spectroscopy (FTIR), for elemental analysis with X-ray photoelectron spectroscopy (XPS), for conductivity with conductive-atomic force microscopy (C-AFM) and the four point probe method. Coatings were formulated with epoxy-polyamide binder system with synthesized pigments at 5 and 20% by weight composition and were applied on the surface of cold rolled steel. The corrosion resistance ability of these coatings was evaluated by constant immersion studies in 5% sodium chloride (NaCl) and corrosion resistance was electrochemically analyzed by electrochemical impedance spectroscopy (EIS) and potentiodynamic polarization techniques.

Experimental work

Materials

For the synthesis of composites, 18.2 MΩ Millipore water was used. TiO_2 (R-702) was obtained from DuPont with alumina as surface treatment. Pristine TiO_2 had a particle size in the range of 200–300 nm. The dopant sodium tungstate dihydrate was purchased from MP Biomedicals, LLC. The oxidant ammonium persulfate (APS) was obtained from EMD Chemicals Inc. The pyrrole was purchased from Alfa Aesar Co. and was distilled prior to use. High purity grade monomer aniline was obtained from Sigma-Aldrich Corporation and was used without any purification. Hydrochloric acid was procured from BDH. For the coating application, cold rolled steel ($0.032'' \times 6'' \times 3''$) panels were procured from Q-Panel Lab Products. Epoxy resin (EPON 828) and polyamide curing agent (EPIKURE 3175) were supplied by Momentive Specialty Chemicals Inc. Methyl ethyl ketone (MEK) was used as a solvent for coating application and was procured from Alfa Aesar Co.

Synthesis of TiO_2/PPy composite and TiO_2/PPy (tungstate doped) composite

For the synthesis of TiO_2/PPy composite, the TiO_2 pigment was soaked in pyrrole monomer for 5 days at ambient temperature. After 5 days of soaking, it was centrifuged (8000 rpm for 15 min) to separate TiO_2 and then this TiO_2 was added to the Erlenmeyer flask containing magnetic stir bar. This was followed by addition of 18.2 MΩ Millipore water to the flask. After proper dispersion of TiO_2 in the water, APS was added and the reaction was continued for 24 h. The product was filtered and washed with an abundant amount of water. Washed product was dried in an oven overnight at 60°C followed by grinding in mortar and pestle. In the end, the product was sieved with sieve #400 of 38 μm opening diameter and was stored in a dry place.

For the preparation of TiO_2/PPy composite (tungstate doped), dopant sodium tungstate dihydrate was added to 18.2 MΩ Millipore water in the above procedure just before the addition of centrifuged and separated TiO_2 to the Erlenmeyer flask. The rest of the procedure and materials were the same as in the above mentioned synthesis of TiO_2/PPy composite. Quantities of all the ingredients used for the synthesis are mentioned in Table 1.

Synthesis of TiO_2/PANI composite

For the synthesis of the TiO_2/PANI composite, TiO_2 pigment was soaked in aniline monomer for 5 days at ambient temperature. After 5 days of soaking, the sample was centrifuged and separated TiO_2 was added to the Erlenmeyer flask containing magnetic stir bar. This was followed by addition of 18.2 MΩ Millipore water to the flask. Prior to addition of water to the flask it was acidified with the hydrochloric acid. After dispersion of TiO_2 in the water, the oxidant APS was added and the reaction was continued for 24 h. The reaction product was filtered and washed with copious amounts of water. This product was dried in oven overnight at 60°C followed by grinding in mortar and pestle. Finally, the product was sieved with sieve #400 of 38 μm opening diameter and was stored at dry place.

Coatings preparation

Prior to the coating's application, cold rolled steel panels were sandblasted with 100 μm alumina grit. Hexane was used for the degreasing of the substrate. At stoichiometric ratio of 1:1 of EPON 828 and EPIKURE 3175, coatings were formulated with 5% and 20% by weight of TiO_2, TiO_2/PPy composite, TiO_2/PPy composite (tungstate doped), and TiO_2/PANI composite. MEK was used as solvent to achieve application viscosity. Coatings were applied with a drawdown bar with wet film thickness of 8 mils. Curing was performed in an oven for 2 h at 80°C. For complete curing of the samples, they were kept at room temperature for 8 days. Formulated coatings are denoted by acronyms as presented in Table 2.

Composite and coatings characterization

JSM-6490LV SEM (JEOL) and JEM-2100 TEM (JEOL) were employed for characterization of the morphology of the synthesized composites. NICOLET 8700 spectrophotometer (Thermo Scientific) was employed for the FTIR characterization. SSX-100 system (Surface Science Laboratories, Inc.) was used for XPS analysis of the composites. A Veeco Dimension 3100 atomic force microscope was employed for CAFM analysis of composite samples. A four point probe instrument consisting of Signatone® probes, a Keithley® 220 programmable current source, and Keithley® 2000 multimeter was employed for the conductivity measurements of the composites. For performing EIS, Gamry Reference 600 Potentiostats with Gamry Framework Version 5.58/EIS 300 software (Gamry Instruments) was used with AC perturbation of 10 mV over the frequency range of 100,000–0.01 Hz at 10 points/decade. EIS was performed with three electrode cell with saturated calomel as a reference electrode, coated substrate as working electrode, and platinum mesh as a counter electrode. Surface area for the EIS measurement was 7.1 cm^2. Potentiodynamic experiments were performed by using same setup as the EIS.

Table 1: Synthesis reactions for composite pigments

Ingredients	TiO_2/PPy composite	TiO_2/PPy (tungstate doped) composite	TiO_2/PANI composite
Pyrrole	30 mL	30 mL	–
Aniline	–	–	30 mL
TiO_2	3 g	3 g	3 g
Hydrochloric Acid	–	–	0.36 g
Water (18.2 MΩ Millipore®)	100 mL	100 mL	100 mL
Sodium tungstate dihydrate	–	1.83 g	–
Ammonium persulfate	2.28 g	2.28 g	2.28 g

Table 2: Formulated coatings with acronyms

Coating	Designation
Coating with 5 wt% of TiO_2	T5
Coating with 20 wt% of TiO_2	T20
Coating with 5 wt% of TiO_2/PPy composite	TiPPy5
Coating with 20 wt% of TiO_2/PPy composite	TiPPy20
Coating with 5 wt% of tungstate doped TiO_2/PPy composite	TiPPyW5
Coating with 20 wt% of tungstate doped TiO_2/PPy composite	TiPPyW20
Coating with 5 wt% of TiO_2/PANI composite	TiPANI5
Coating with 5 wt% of TiO_2/PANI composite	TiPANI20

Results and discussion

Morphology

All the mentioned composites (TiO_2/PPy composite, TiO_2/PPy (tungstate doped) composite, and TiO_2/PANI composite) were synthesized in situ with single step chemical oxidative polymerization. SEM micrographs of TiO_2, TiO_2/PPy composite, TiO_2/PPy (tungstate doped) composite, and TiO_2/PANI composite are shown in Fig. 1. All of the micrographs were obtained at the same magnification and accelerating voltage, which are mentioned on each micrograph. As observed in Fig. 1, TiO_2 as such is spherical and well separated without any agglomeration with a particle size of individual particles in the range of 200–300 nm. In the case of the TiO_2/PPy composite, an increase in the particle size of the particles was observed with varied particle size distribution and greater agglomeration. The observed morphology was also not spherical as in the case of just TiO_2. For the TiO_2/PPy (tungstate doped) composite, a greater degree of agglomeration was observed, possibly due to the presence of tungstate dopant. The nature and concentration of dopant in the synthesis of CPs result in order or disorder in the morphology of the CPs formation.[57] In the case of the TiO_2/PANI composite, an even larger amount of agglomeration was observed.

TEM images of TiO_2, TiO_2/PPy composite, TiO_2/PPy (tungstate doped) composite, and TiO_2/PANI composite are shown in Fig. 2. For the as-received TiO_2 as observed in Fig. 2, spherical and needle-like morphology was observed. For TiO_2/PPy composite, uniform thickness layer of PPy was observed around TiO_2 particles exhibiting core and shell morphology. This is the unique core and shell morphology of TiO_2/PPy synthesized in a very facile manner. The average thickness of PPy shell was 50–60 nm around TiO_2 particles. Incorporation of PPy also resulted in agglomeration. In the case of TiO_2/PPy (tungstate doped) composite, a much more dense layer of PPy was formed around TiO_2 particles. The average thickness of PPy shell was 80–100 nm around TiO_2 particles and the growth of PPy particles was also denser than that with the TiO_2/PPy composite. The compactness of PPy in the formation was found to be affected by the incorporation of the dopant anion.[58] For the TiO_2/PANI composite, PANI was randomly distributed around TiO_2 particles without any definite final morphology of TiO_2/PANI composite. Agglomerated morphology was also evident for the TiO_2/PANI composite, as observed in Fig. 2. Even though the resultant composite observed as agglomerated solids, size of agglomerates was small, resulting in free flowing particles which could be easily incorporated into the coatings.

Chemical composition

The elemental composition was obtained by XPS analysis, as shown in Fig. 3. As observed in Fig. 3, with the as-received TiO_2 pigment particles, titanium, oxygen, and aluminum content was high as compared to the TiO_2/PPy composite, TiO_2/PPy (tungstate doped) composite, and TiO_2/PANI composite. The presence of aluminum in the case of TiO_2 pigment particles was attributed to the alumina surface treatment.

The presence of nitrogen in the case of the TiO_2/PPy composite, TiO_2/PPy (tungstate doped) composite indicated formation of PPy and in the case of the TiO_2/PANI composite indicated the formation of PANI. The presence of sulfur in the case of TiO_2/PPy composite and TiO_2/PANI composite indicated sulfur doping whereas the presence of tungsten with the TiO_2/PPy (tungstate doped) composite indicated doping by tungsten anion. In the case of TiO_2/PPy composite and TiO_2/PANI composite, the presence of sulfur can be attributed to the doping due to sulfate

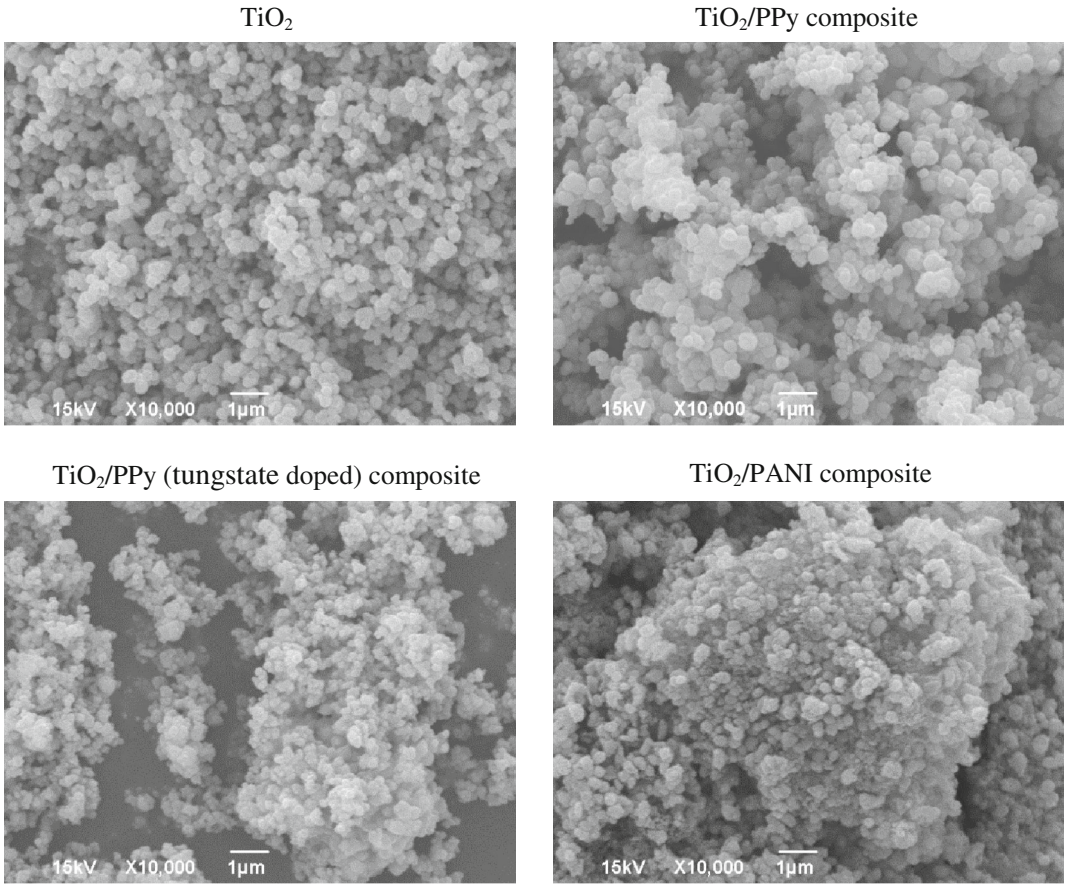

Fig. 1: SEM micrographs of TiO_2 (top left), TiO_2/PPy composite (top right), TiO_2/PPy (tungstate doped) composite (bottom left), and TiO_2/PANI composite (bottom right)

anion arising from the oxidant APS. No sulfur or very minimal sulfur was detected with the TiO_2/PPy (tungstate doped) composite probably due to the possible competition by tungstate dopant for incorporation on PPy backbone. More titanium was observed in case of TiO_2/PANI composite, indicating bare particles of TiO_2 adjacent to the matrix of PANI. This morphology can be confirmed with the TEM image, as shown in Fig. 2 (bottom right). No titanium was observed in the case of TiO_2/PPy (tungstate doped) composite, indicating TiO_2 particles completely encapsulated in the PPy matrix, as observed in the TEM image (Fig. 2 (bottom left)). The ratios of dopant to nitrogen were obtained from the elemental analysis. For the TiO_2/PPy composite, S/N ratio was 0.21, for TiO_2/PPy (tungstate doped) composite, the W/N ratio was 0.14, and for TiO_2/PANI composite, S/N ratio was 0.23.

High resolution core level spectrum of N 1s was obtained for TiO_2/PPy composite (Fig. 4), TiO_2/PPy (tungstate doped) composite (Fig. 5), and TiO_2/PANI composite (Fig. 7), whereas high resolution core level spectrum of W 4f was obtained for (tungstate doped) composite (Fig. 6). The spectra for N 1s and W 4f were deconvulated into the individual peaks and are tabulated in Table 3.

The respective percentages of obtained species are also mentioned in Table 3. In the case of the TiO_2/PPy composite, the peak at 398.02 eV was ascribed to imine nitrogen (–N=),[59] the peak at 399.90 eV was attributed to neutral amine nitrogen (–NH–), and the peak at 401.19 eV was ascribed to positively charged nitrogen atom ($–N^+–$).[60] With the TiO_2/PPy (tungstate doped) composite, the neutral amine nitrogen (–NH–) and positively charged nitrogen atom ($–N^+–$) were found at 400.21 and 401.25 eV, respectively. For the TiO_2/PPy (tungstate doped) composite, a deconvulated W 4f spectrum showed peaks at 35.68, 37.80, and at 41.3 eV. For this, 35.68 and 37.80 eV correspond to W^{6+} oxidation state[52,61] and the 41.3 eV is a peak due to W loss. In the case of TiO_2/PANI composite, 398.50 eV peak was attributed to imine nitrogen (–N=), 400.25 eV peak due to the localized positively charged nitrogen ($–N^+–$), and at 401.56 eV, due to the positively charged nitrogen atom ($–N^+–$).[62] Protonation level can be obtained by $[N^+]/[N]$ ratio.[63] Higher level of protonation signified higher doping for the composite pigments.

FTIR spectra was obtained for TiO_2, TiO_2/PPy composite, TiO_2/PPy (tungstate doped) composite, and TiO_2/PANI composite and is shown in Figs. 8a–8d).

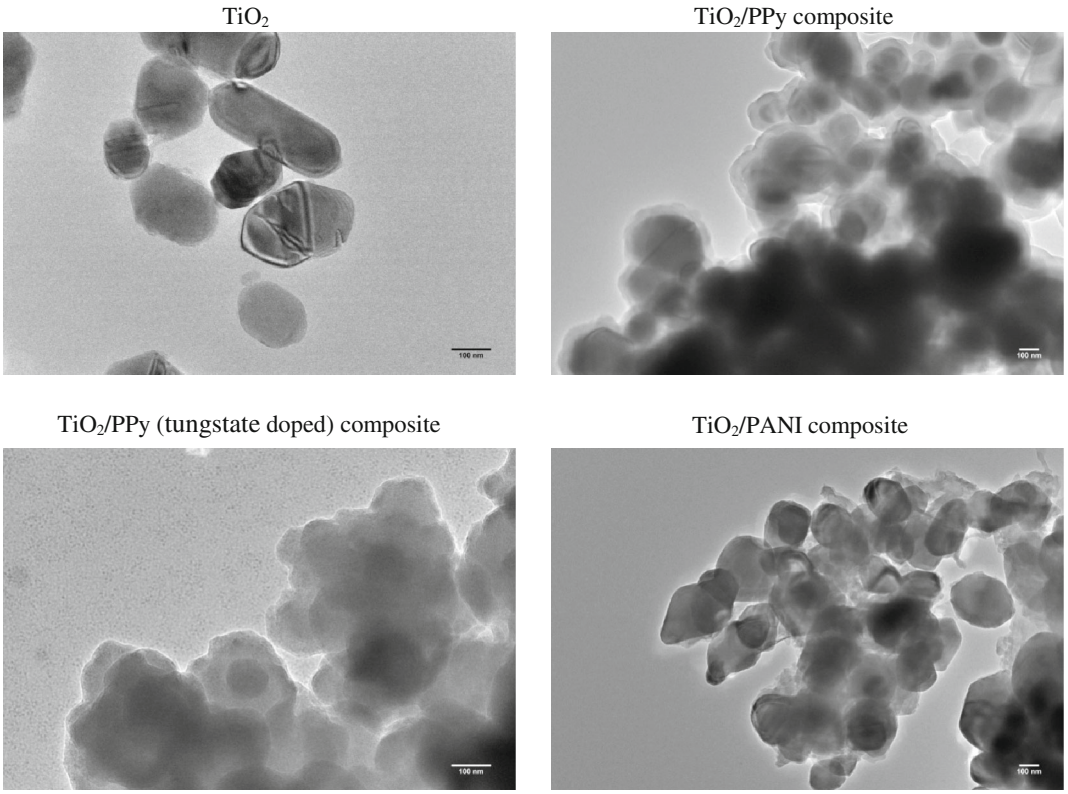

Fig. 2: TEM images of TiO_2 (top left), TiO_2/PPy composite (top right), TiO_2/PPy (tungstate doped) composite (bottom left), and TiO_2/PANI composite (bottom right)

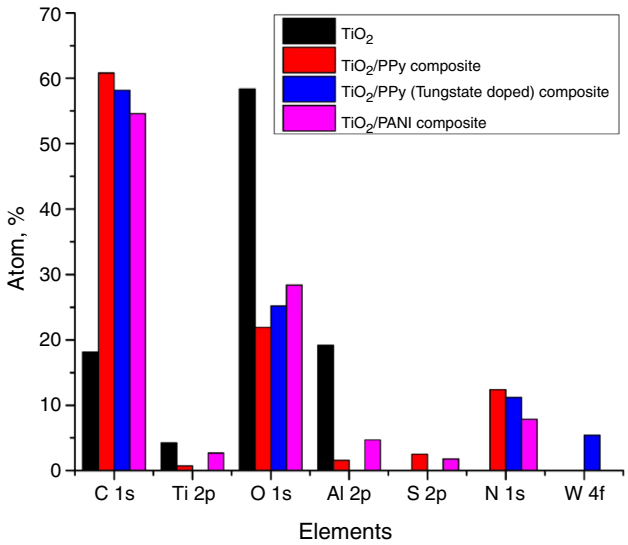

Fig. 3: Elemental composition obtained by XPS

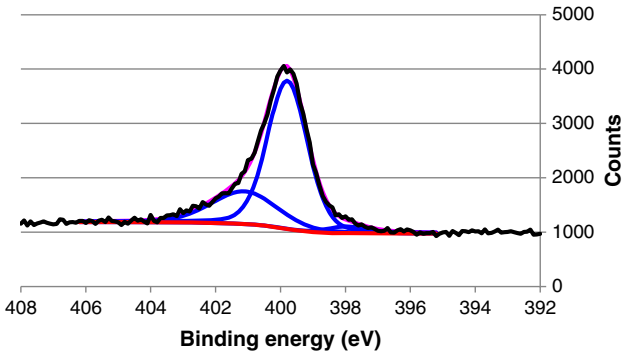

Fig. 4: TiO_2/PPy composite N 1s high resolution

Respective wavenumbers (cm^{-1}) and modes of vibration are presented in Table 4. The TiO_2 absorption band[64] can be found at 700–500 cm^{-1} as observed in Fig. 8a. This peak for TiO_2 was overshadowed by other characteristic peaks for PPy in the case of the TiO_2/PPy composite (Fig. 8b), PPy and tungstate ion band in the case of TiO_2/PPy (tungstate doped) composite (Fig. 8c), and by PANI characteristic bands for the TiO_2/PANI composite (Fig. 8d). This may be due to the possible interaction of the PPy or PANI or tungstate ion with the TiO_2 surface.[65]

The carbonyl group vibration band for TiO_2/PPy composite and TiO_2/PPy (tungstate doped) composite was observed at 1701 cm^{-1} due to overoxidation of CPs, but this band was not very prominent in both of the cases, suggesting minimal loss in conductivity.[66] C–C and C=C ring stretching vibrations were observed at 1561 and 1558 cm^{-1} in the TiO_2/PPy composite

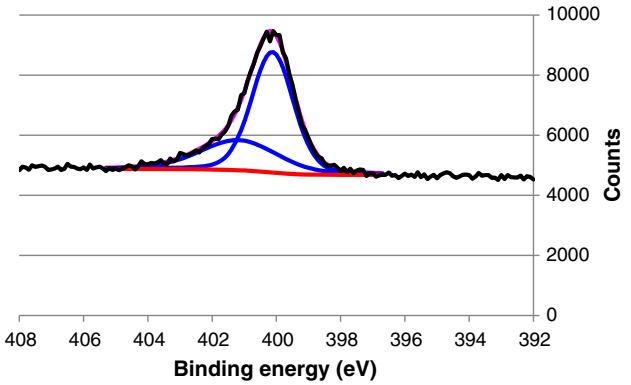

Fig. 5: TiO_2/PPy (tungstate doped) composite N 1s high resolution

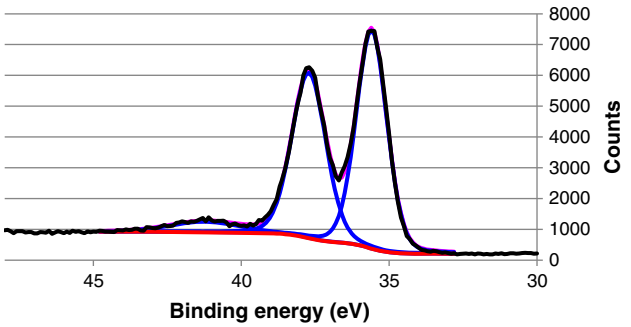

Fig. 6: TiO_2/PPy (tungstate doped) composite, W 4f high resolution

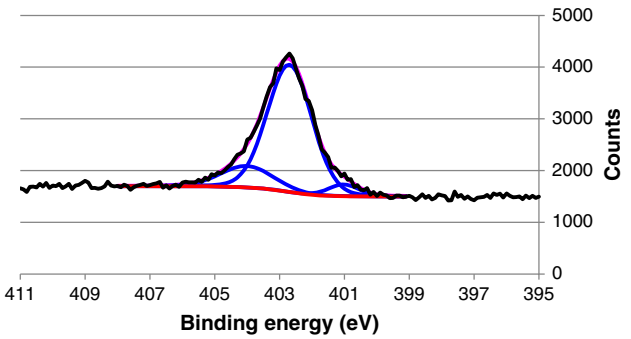

Fig. 7: TiO_2/PANI composite N 1s high resolution

and the TiO_2/PPy (tungstate doped) composite, respectively. C–N and C=C stretching vibrations were observed at 1473 and 1463 cm^{-1} for TiO_2/PPy composite and TiO_2/PPy (tungstate doped) composite, respectively.[67] C–H and C–N in plane deformations (1311 cm^{-1}) were observed for TiO_2/PPy composite and TiO_2/PPy (tungstate doped) composite.[68] Pyrrole ring breathing vibration was observed at 1202 and 1199 cm^{-1} for TiO_2/PPy composite and TiO_2/PPy (tungstate doped) composite, respectively.[69] Vibrations at around 1090 cm^{-1} (C–C in plane deformation) and 1045 cm^{-1} (C–H deformation) were observed in both the TiO_2/PPy composite and the TiO_2/PPy (tungstate doped) composite.[70] PPy characteristic peak at 929 and 788 cm^{-1} were also observed for TiO_2/PPy composite and TiO_2/PPy (tungstate doped) composite. Tungstate ion band 960–780 and 900–770 cm^{-1} was observed for TiO_2/PPy (tungstate doped) composite as observed in Fig. 8c.[64]

For the TiO_2/PANI composite, the band at 1581 cm^{-1} was observed due to quinoid stretching vibration mode and at 1501 cm^{-1} due to the benzenoid unit, as seen in Fig. 8d.[71–73] The band at 1458 cm^{-1} is due to the benzene ring deformation [74] which was observed at 1448 cm^{-1} for the TiO_2/PANI composite. The band at 1299 cm^{-1} was observed due to the C–N stretching mode indicating the protonation of PANI.[52] The band at 1235 cm^{-1} is due to the C–C twisting and was observed at 1229 cm^{-1} as seen in Fig. 8d.[75] The band at 1144 cm^{-1} is due to $-NH^+=$ vibration resulting from protonation and was observed at 1148 cm^{-1} for TiO_2/PANI composite.[52] The band at 1045 cm^{-1} is due to C–H in plane bending mode and was observed at 1042 cm^{-1}.[72]

Conductivity

For surface conductivity, CAFM experiments were performed on the pressed pellets of composites glued to the aluminum mounts. For the CAFM measurements, 100 mV DC bias was applied. Surface topography, deflection, and current images for TiO_2/PPy composite, TiO_2/PPy (tungstate doped) composite, and TiO_2/PANI composite are presented in Figs. 9, 10, and 11, respectively. As observed in Fig. 9, the current image illustrated dense current density for the TiO_2/PPy composite, whereas for TiO_2/PPy (tungstate doped) composite (Fig. 10) current image exhibited less dense areas as compared to the TiO_2/PPy composite. For TiO_2/PANI composite (Fig. 11), the current image did not exhibit significant current density. The conductive regions in CAFM measurements are on local scale so the current density image shows the local conductive representation whereas for global scale conductivity measurements were gathered by four point conductivity measurements. The same pellets as used for CAFM measurements were employed in four point probe conductivity measurements and the results are presented in Fig. 12. The TiO_2/PPy (tungstate doped) composite showed the highest conductivity which might be possible due to the doping of tungstate ion in the backbone of PPy. Again here, the conductivity of the composite material is measured which gets affected by the presence of TiO_2 in the total matrix. Even though the XPS results suggest that the TiO_2/PANI composite will be conductive, because of its presence in the blend with TiO_2 a decrease in the conductivity results. There is also the possibility that in the TiO_2/PANI composite, the presence of TiO_2 is such that connectivity between PANI chains is not achieved and so lesser conductivity is observed or the amount of PANI is not enough to provide high

Table 3: Peak distribution for composites obtained by XPS

TiO_2/PPy composite			TiO_2/PPy (tungstate doped) composite			TiO_2/PANI composite		
Peak (eV)	Species	Group (%)	Peak (eV)	Species	Group (%)	Peak (eV)	Species	Group (%)
398.02	–N= imine nitrogen	3.03	400.21	–NH– neutral amine nitrogen	68.67	398.50	–N= imine nitrogen	5.04
399.90	–NH– neutral amine nitrogen	71.44	401.25	$–N^+–$ positively charged nitrogen atom	31.33	400.25	$–N^+–$ localized positively charged nitrogen atom	79.27
401.19	$–N^+–$ positively charged nitrogen atom	25.53	35.68	W $4f_{7/2}$ W^{6+} oxidation state	51.16	401.56	$–N^+–$ positively charged nitrogen atom	15.69
			37.80	W $4f_{5/2}$ W^{6+} oxidation state	43.21			
			41.30	W loss peak	5.63			

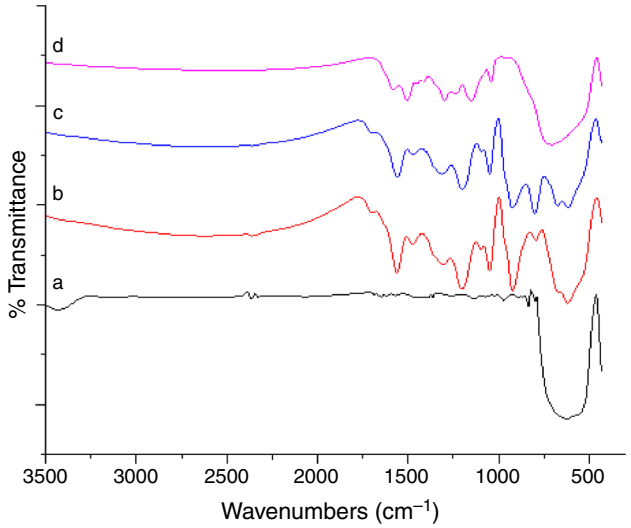

Fig. 8: FTIR spectra of (a) TiO_2, (b) TiO_2/PPy composite, (c) TiO_2/PPy (tungstate doped) composite, and (d) TiO_2/PANI composite

conductivity.[76] Conductivity value of TiO_2/PANI composite is 2.224×10^{-5} S m^{-1}. It has been observed that charge transport in PANI composites depends on the PANI percentage in the total composite as well.[77]

Electrochemical impedance spectroscopy (EIS)

EIS is a powerful technique which has been employed for studying corrosion protection provided by coatings.[78–81] EIS was performed on the coated samples immersed in the 5% NaCl at initial, 24 h, 7 days, 14 days, and 21 days. Bode plot of T5 and T20, TiPPy5 and TiPPy20, TiPPyW5 and TiPPyW20, TiPANI5 and TiPANI20 are presented in Figs. 13, 14, 15, and 16, respectively. For coating T5 (Fig. 13 (left)), initial impedance (low frequency) was very high but as the duration of exposure to the electrolyte increased (21 days), the value of low frequency impedance decreased to lower than 10^5 Ω indicating passage of electrolyte through the coating and reaching the interface, leading to corrosion. In the case of T20 coating (Fig. 13 (right)), low frequency impedance which was higher initially decreased to 10^8 Ω as exposure duration to the electrolyte increased to 21 days. In the case of TiPPy5 and TiPPy20 (Fig. 14), the initial value of low frequency impedance was 10^8 Ω; however, after 21 days of exposure to the electrolyte, only an order of magnitude decrease to 10^7–10^6 Ω was observed. For TiPPyW5 (Fig. 15 (left)), initial low frequency impedance decreased to 10^8 Ω after electrolyte exposure for 21 days, whereas for TiPPyW20 (Fig. 15 (right)), it reached a value of 10^9 Ω. In the case of TiPANI5 and TiPANI20 (Fig. 16), after 21 days of exposure by constant immersion in the electrolyte, the value of low frequency impedance was decreased to 10^9 Ω. As observed in Figs. 15 and 16, initial low frequency impedance values

Table 4: Peak positions (cm^{-1}) and FTIR modes of vibrations for TiO_2, TiO_2/PPy composite, TiO_2/PPy (tungstate doped) composite, and TiO_2/PANI composite

Wavenumbers (cm^{-1}) and modes of vibration	TiO_2 [Wavenumber (cm^{-1})]	TiO_2/PPy composite [Wavenumber (cm^{-1})]	TiO_2/PPy (tungstate doped) composite [Wavenumber (cm^{-1})]	TiO_2/PANI composite [Wavenumber (cm^{-1})]
1702, carbonyl group		1701	1701	
1580, quinoid stretching				1581
1558, C–C and C=C ring stretching		1561	1558	
1501, benzenoid unit				1505
1464, C–N and C=C stretching		1473	1463	
1458, benzene ring deformation				1448
1300, C–N stretching mode				1299
1295, C–H and C–N in plane deformation		1311	1311	
1229, C–C twisting				1229
1144, $–NH^+=$ vibration due to protonation				1148
1198, ring breathing		1202	1199	
1090, C–C in plane deformation		1090	1090	
1045, C–H deformation		1048	1049	
1045, C–H in plane bending				1042
929 and 788 PPy characteristic peak, 700–660 TiO_2 peaks, 960–780 and 900–770 tungstate ion band	700–500	923, 792, 678, 616	925, 801, 678, 617	707

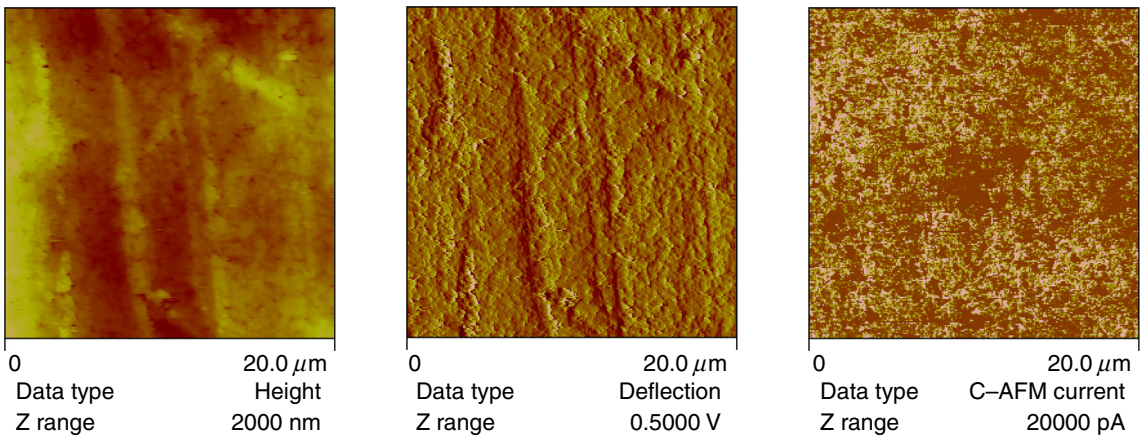

Fig. 9: Height, deflection, and current images for TiO_2/PPy composite

were very high (10^{10}–10^{11} Ω); however, as exposure duration to the electrolyte increased, the impedance was observed to decrease.

ZView2 software from Scribner® Associates Inc. was employed for the equivalent circuit modeling and fitting of the EIS data. The circuit models used for the data fitting are shown in Fig. 17, and the circuit element fit results are presented in Table 5. In Fig. 17, R1 is solution resistance, R2 is coating resistance, R3 is polarization resistance, Cc is coating capacitance, Cdl is double layer capacitance, and Ws is Warburg short element. Constant phase element

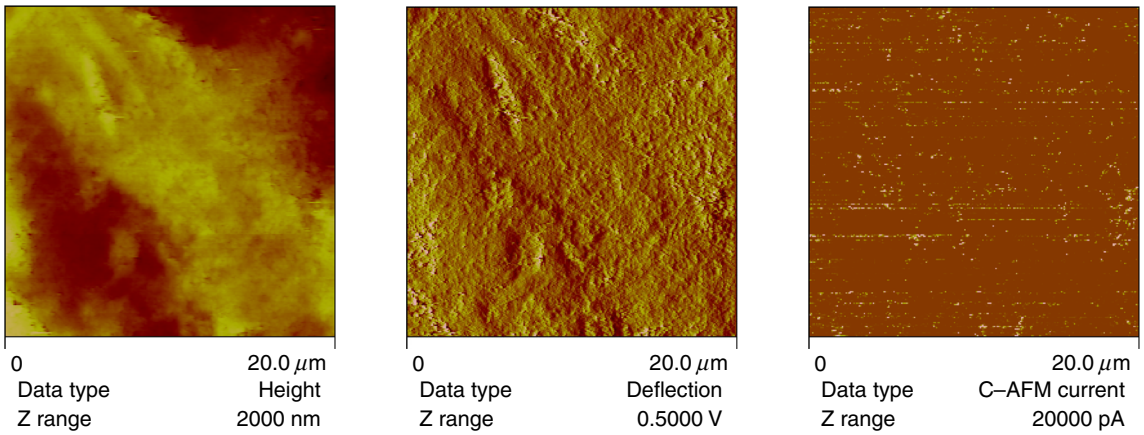

Fig. 10: Height, deflection, and current images for TiO_2/PPy (tungstate doped) composite

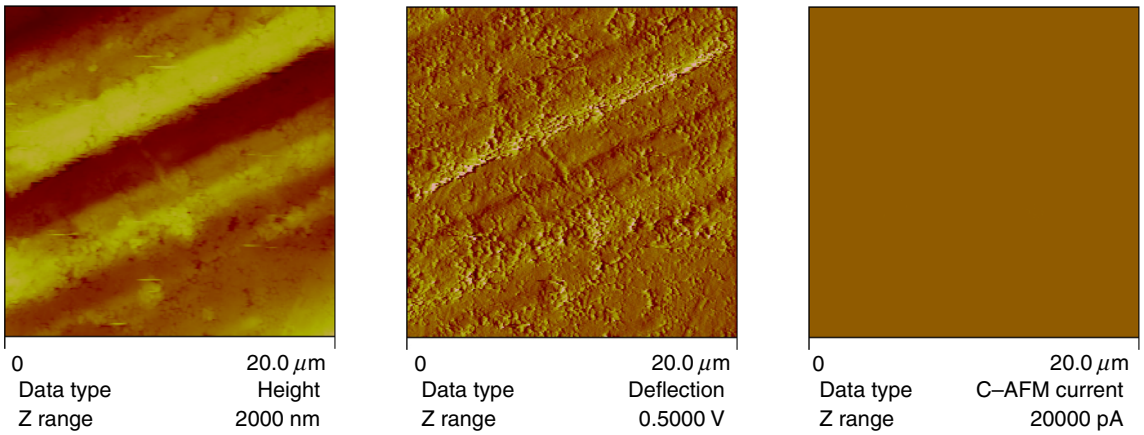

Fig. 11: Height, deflection, and current images for TiO_2/PANI composite

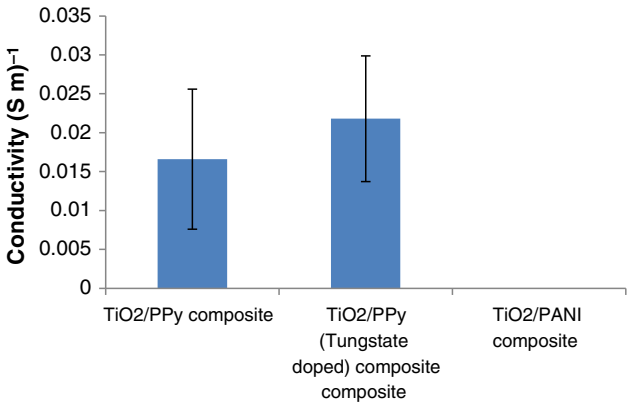

Fig. 12: Conductivity values obtained by four point probe measurement

(CPE) is a pseudo capacitor. Its impedance of CPE can be obtained by equation (1).[54,82]

$$Z_{(\mathrm{CPE})} = 1/\left[(T)(j\omega)^{P}\right], \tag{1}$$

where T is capacitance, j is an imaginary component, ω is the angular frequency ($\omega = 2\pi f$, f is the frequency), P is the power ($0 \leq n \leq 1$), and $Z_{(\mathrm{CPE})}$ is the impedance of CPE. P value close to 1 represents capacitor behavior. Diffusion phenomena observed in the coatings as time of immersion in electrolyte increased was modeled by employing equation (2).[82]

$$Z_{\mathrm{w}} = 1/\sigma(i\omega)^{(-1/2)}, \tag{2}$$

where Z_{w} is Warburg impedance, i is imaginary component, σ is Warburg capacitance, and ω is the angular frequency.

For coating T5, after 24 h of immersion in electrolyte, a second time constant was observed in Bode plot (Fig. 13 (left)). Second time constant continued for 14 days and this data was modeled by circuit model presented in Fig. 17b. At the 21st day, there was a possibility of a second time constant in the low frequency region but, due to noise, it was difficult to model. There is a possibility of complete damage of the coating due to the immersion.[46] This was also sup-

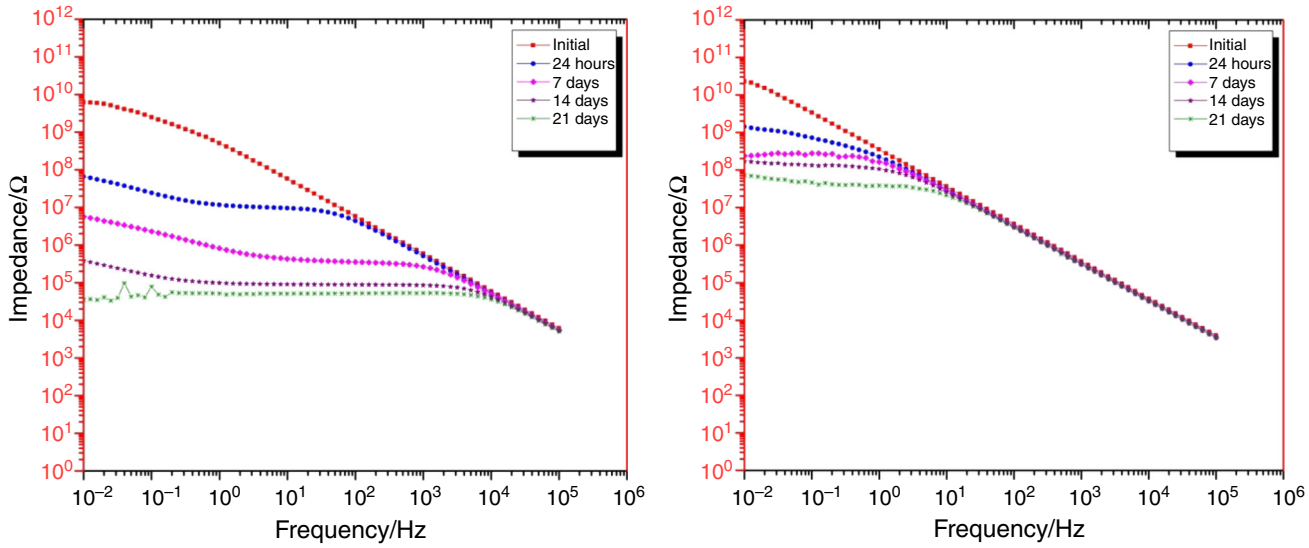

Fig. 13: Bode plot of T5 (left) and T20 (right)

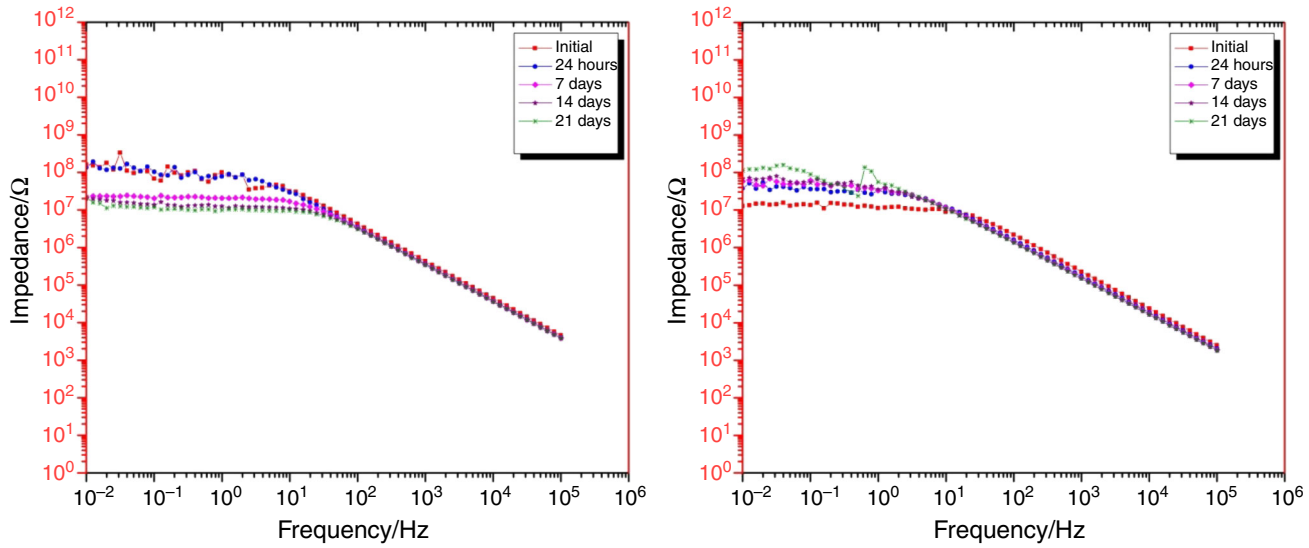

Fig. 14: Bode plot of TiPPy5 (left) and TiPPy20 (right)

ported with the lower impedance observed at low frequency obtained from circuit modeling (10^4 Ω) (Table 5). The increase in the capacitance value ($CPE_{dl} - T$) suggested the coatings degradation as exposure to the electrolyte increased. Increase in $CPE_{dl} - T$ value with immersion time was also observed in the case of coating T20 (Table 5); however, this increase was not significant as compared to coating T5.

For coating TiPPy5, coating resistance (Rc) steadily decreased as exposure time to the electrolyte increased; however, at the same time, a second time constant also appeared at the 14th and 21st day of immersion, indicating corrosion happening underneath the coating upon the substrate.[83] For coating TiPPy20, coatings resistance (Rc), increased at the 21st day of immersion, indicating formation of a passive layer due to the corrosion production or the passivation achieved by PPy underneath the coating.[28,84] For coatings TiPPyW5 and TiPPyW20, the drop in the value of Rc was followed by an increase in the value of Rc at the 21st day of immersion. A similar observation was made on the mild steel substrate coated with tungstate doped PPy. The tungstate anion participated in the passivation process, resulting in an increase in coating resistance value.[35] Increase in the values of polarization resistance (Rct) also suggested an increase in charge transfer resistance in tungstate-doped coatings.

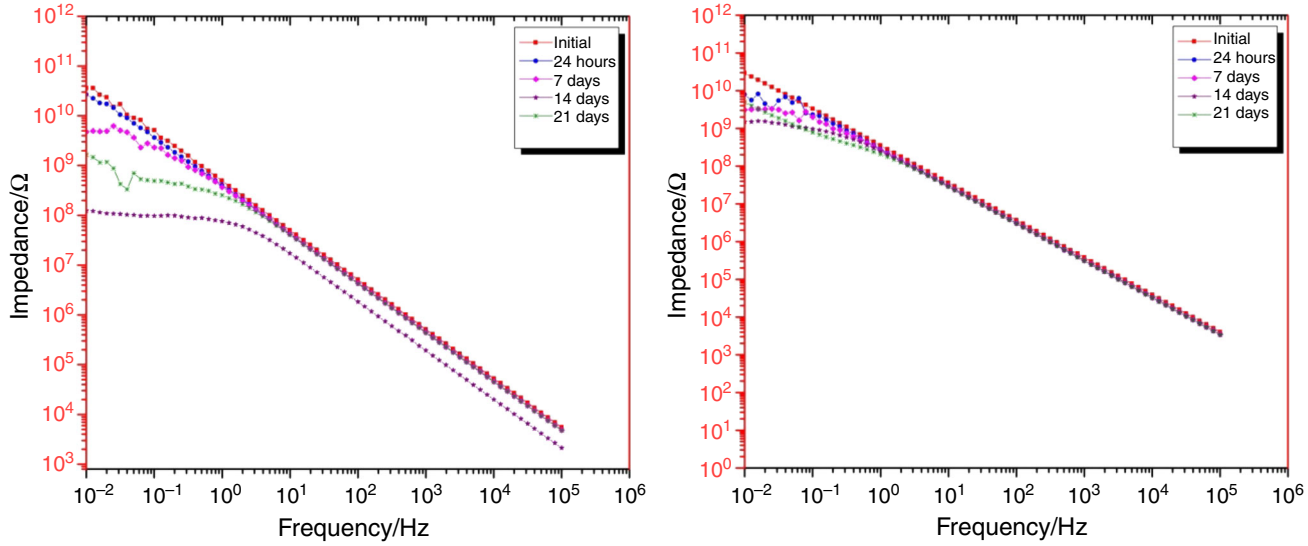

Fig. 15: Bode plot of TiPPyW5 (left) and TiPPyW20 (right)

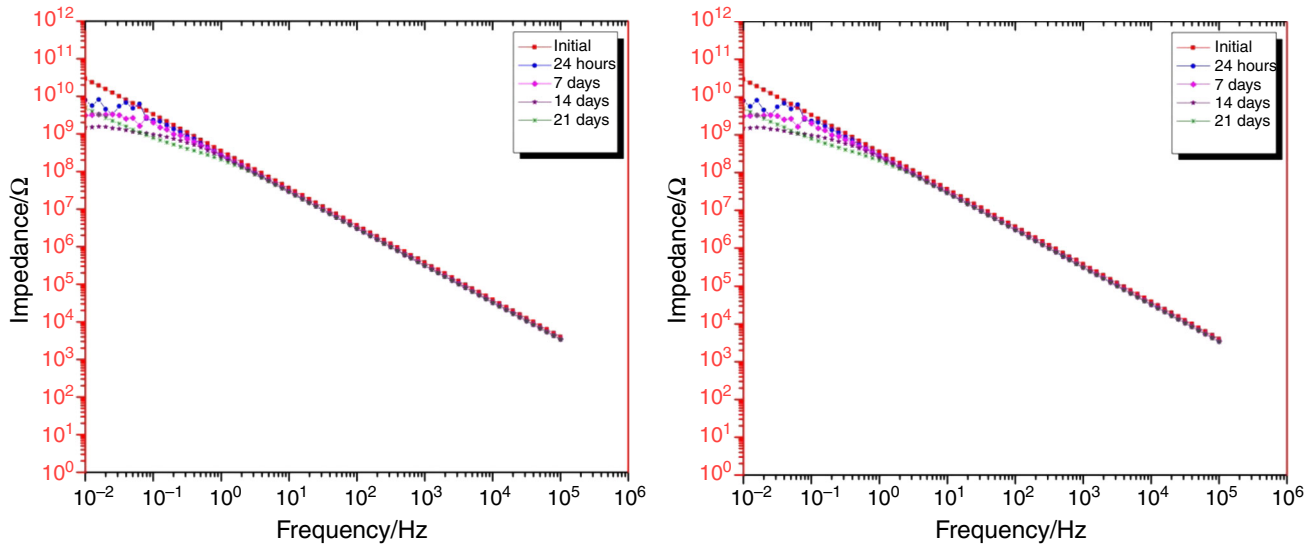

Fig. 16: Bode plot of TiPANI5 (left) and TiPANI20 (right)

For the TiPANI5 coating, Warburg element appeared at the 24 h and 7th day, indicating the diffusion of species through the coating; however, at the 14th and 21st day, a second time constant appeared suggesting a reaction occurring at the interface of the metal and the coating. However, the coating resistance value was still at 10^7 Ω after 21 days of immersion. For the TiPANI20 coating, only one time constant was employed for modeling the data and coating resistance at 21st day of immersion was still high. Protection mechanism suggested for the protection of mild steel substrate by PANI is mostly passivation resulting from the redox activity.[85]

Potentiodynamic scans

Potentiodynamic scans were performed on the defect made up of size 1.5 cm in length and 1 mm in width. For T5, T20, TiPPy5, TiPPy20, TiPPyW5, TiPPyW20, TiPANI5, and TiPANI20, potentiodynamic scans are shown in Fig. 18. The corrosion potential was shifted in a positive direction by 100–200 mV for all of the coating systems as compared to T5 and T20. Almost a 250 mV positive shift in potential was obtained for TiPPyW20. This might be due to the increase in storage charge in TiPPyW20 coating due to tungstate ion incorporation, resulting in improved corrosion

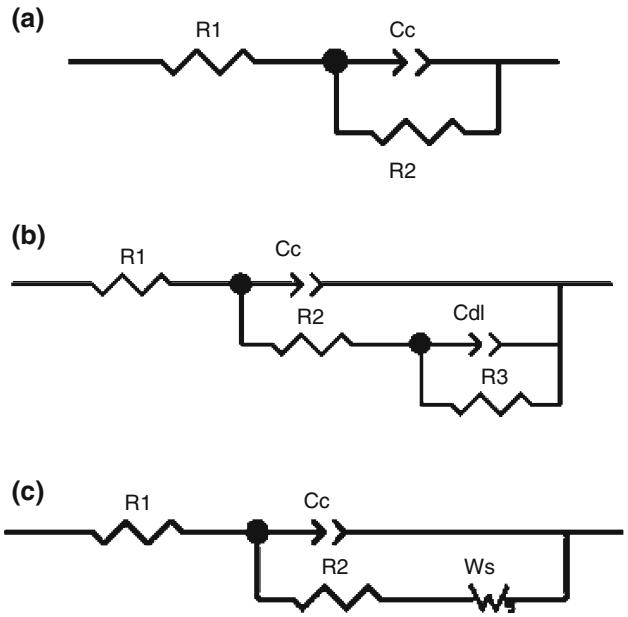

Fig. 17: Equivalent circuit models for EIS data fitting

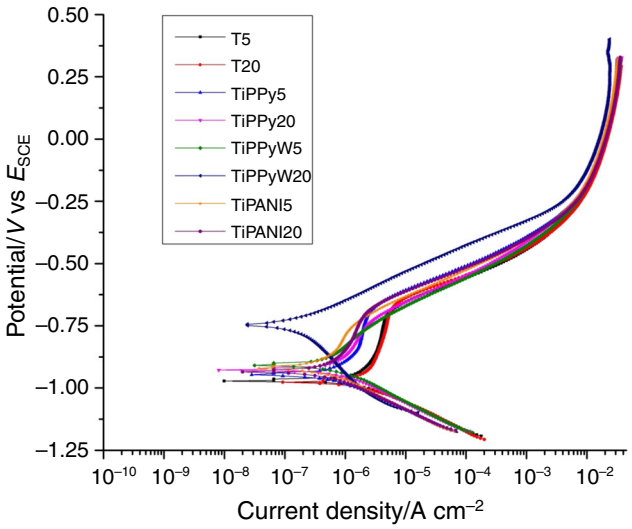

Fig. 18: Potentiodynamic scans

Table 5: Fit results obtained from equivalent circuit modeling of EIS data

	Time	Rc (Ω)	CPEc		Rct (Ω)	W–R (Ω)	CPEdl	
			T (F)	*P*			*T* (F)	*P*
T5	Initial	5.28×10^{9}	3.55×10^{-10}	0.97				
	24 h	9.44×10^{6}	3.48×10^{-10}	0.99	1.31×10^{8}		7.48×10^{-8}	0.68
	7 days	3.32×10^{5}	4.21×10^{-10}	0.97	9.46×10^{6}		5.60×10^{-7}	0.60
	14 days	8.81×10^{4}	4.55×10^{-10}	0.97	5.30×10^{6}		1.47×10^{-5}	0.69
	21 days	5.31×10^{4}	3.49×10^{-10}	0.99				
T20	Initial	8.21×10^{10}	4.79×10^{-10}	0.99				
	24 h	2.91×10^{8}	5.57×10^{-10}	0.98	2.21×10^{9}		1.78×10^{-9}	0.49
	7 days	1.19×10^{8}	5.88×10^{-10}	0.98	1.58×10^{8}		1.06×10^{-9}	0.63
	14 days	1.26×10^{8}	6.78×10^{-10}	0.97				
	21 days	3.73×10^{7}	6.38×10^{-10}	0.98	3.88×10^{7}		9.06×10^{-8}	0.71
TiPPy5	Initial	1.20×10^{8}	5.07×10^{-10}	0.97				
	24 h	1.14×10^{8}	6.05×10^{-10}	0.97				
	7 days	2.18×10^{7}	5.75×10^{-10}	0.97				
	14 days	1.20×10^{7}	5.61×10^{-10}	0.97	1.14×10^{7}		3.49×10^{-7}	0.56
	21 days	9.97×10^{6}	5.62×10^{-10}	0.97	6.78×10^{6}		6.44×10^{-7}	0.81
TiPPy20	Initial	1.28×10^{7}	8.51×10^{-10}	0.98				
	24 h	3.52×10^{7}	1.37×10^{-9}	0.96				
	7 days	4.93×10^{7}	1.72×10^{-9}	0.94				
	14 days	5.80×10^{7}	1.95×10^{-9}	0.93				
	21 days	1.15×10^{8}	2.04×10^{-9}	0.94				
TiPPyW5	Initial	7.06×10^{10}	3.27×10^{-10}	0.99				
	24 h	4.22×10^{10}	4.20×10^{-10}	0.98				
	7 days	5.25×10^{9}	4.63×10^{-10}	0.97				
	14 days	8.40×10^{7}	9.76×10^{-10}	0.98	7.89×10^{7}		5.88×10^{-8}	0.45
	21 days	4.36×10^{8}	4.36×10^{-10}	0.98	8.00×10^{8}		7.55×10^{-9}	1
TiPPyW20	Initial	2.21×10^{11}	4.77×10^{-10}	0.98				
	24 h	8.01×10^{9}	5.60×10^{-10}	0.99				
	7 days	4.01×10^{9}	6.76×10^{-10}	0.97				
	14 days	1.43×10^{9}	6.93×10^{-10}	0.97				
	21 days	4.88×10^{8}	6.03×10^{-10}	0.98	5.87×10^{9}		1.78×10^{-9}	0.86
TiPANI5	Initial	8.25×10^{10}	2.82×10^{-10}	0.99				
	24 h	2.85×10^{7}	3.98×10^{-10}	0.98		2.54×10^{9}		
	7 days	5.70×10^{7}	4.16×10^{-10}	0.98		3.89×10^{8}		
	14 days	4.63×10^{7}	4.19×10^{-10}	0.98	2.27×10^{8}		2.11×10^{-8}	0.17
	21 days	5.03×10^{7}	4.39×10^{-10}	0.97	6.36×10^{7}		6.58×10^{-8}	0.65
TiPANI20	Initial	6.75×10^{10}	5.22×10^{-10}	0.97				
	24 h	1.76×10^{8}	1.86×10^{-9}	0.90				
	7 days	1.04×10^{8}	2.63×10^{-9}	0.87				
	14 days	9.90×10^{7}	2.86×10^{-9}	0.87				
	21 days	1.87×10^{7}	2.70×10^{-9}	0.87				

protection.[86] There is also the possibility of participation in the passivation process by tungstate anion resulting in improved corrosion protection.[51] Due to the core and shell morphology of particles of PPy and TiO_2, effective area for redox activity and for metal surface interaction increased in case of TiO_2/PPy composite.[47] Another mechanism at work is the barrier protection provided by formed passivation layer to the corrosive species. The possibility of combining tungstate with ferrous ions resulting from the oxidation of the underlying steel also results in corrosion protection. Additionally, PPy and PANI are *p*-type material whereas TiO_2 is *n*-type semiconductor which acts as inhibitor to the transport of holes. Intimate contact of CPs with TiO_2 results into the formation of *p*–*n* junction which will decrease the charge transfer, leading to a decrease in the corrosion rate.[46]

Conclusions

The core and shell composite of PPy and TiO_2 was successfully prepared by chemical oxidative polymerization with PPy shell thickness of 50–60 nm. Similar and denser morphology was also obtained for TiO_2/PPy composite doped with tungstate anion. TiO_2/PPy composite and TiO_2/PPy (tungstate doped) composite were found to be conductive, as observed in CAFM and four point probe conductivity measurements. TiO_2/PPy composite, TiO_2/PANI composite, and TiO_2/PPy (tungstate doped) composite-based coatings exhibited improved corrosion protection on steel substrate as evidenced in EIS measurements and potentiodynamic scans. The suggested mechanisms for improved corrosion protection are the effective area increase of CP, passivation, and dopant release.

Acknowledgments The authors gratefully acknowledge the support of this research by US Army Research Laboratory under Grant No. W911NF-09-2-0014, W911NF-10-2-0082, and W911NF-11-2-0027.

References

1. Hays, GF, ''World Corrosion Organization.'' In: Eliezer, A (ed.) *Corrodia*. NACE International, Houston, 2010
2. Sangaj, NS, Malshe, VC, ''Permeability of Polymers in Protective Organic Coatings.'' *Prog. Org. Coat.*, **50** (1) 28–39 (2004)
3. Roberge, P, *Corrosion Engineering: Principles and Practice*. McGraw-Hill Education, New York, 2008
4. McCafferty, E, *Introduction to Corrosion Science*. Springer, New York, 2010
5. Davis, JR, *Corrosion: Understanding the Basics*. ASM International, Materials Park, 2000
6. Ahmad, Z, *Principles of Corrosion Engineering and Corrosion Control*. Elsevier Science, Oxford, 2006
7. Cohen, MD, Kargacin, B, Klein, CB, Costa, M, ''Mechanisms of Chromium Carcinogenicity and Toxicity.'' *Crit. Rev. Toxicol.*, **23** (3) 255–281 (1993)
8. Hong, SY, Marynick, DS, ''Understanding the Conformational Stability and Electronic Structures of Modified Polymers Based in Polythiophene.'' *Macromolecules*, **25** (18) 4652–4657 (1992)
9. Zor, S, Kandemirli, F, Yakar, E, Arslan, T, ''Electrochemical Synthesis of Polypyrrole on Aluminium in Different Anions and Corrosion Protection of Aluminium.'' *Prot. Met. Phys. Chem. Surf.*, **46** (1) 110–116 (2010)
10. Bai, H, Shi, GQ, ''Gas Sensors Based on Conducting Polymers.'' *Sensors*, **7** (3) 267–307 (2007)
11. Smela, E, ''Conjugated Polymer Actuators for Biomedical Applications.'' *Adv. Mater.*, **15** (6) 481–494 (2003)
12. Rudge, A, Davey, J, Raistrick, I, Gottesfeld, S, Ferraris, JP, ''Conducting Polymers as Active Materials in Electrochemical Capacitors.'' *J. Power Sources*, **47** (1–2) 89–107 (1994)
13. Chandrasekhar, P, *Conducting Polymers, Fundamentals and Applications: A Practical Approach*. Springer, New York, 1999
14. Gurunathan, K, Amalnerkar, DP, Trivedi, DC, ''Synthesis and Characterization of Conducting Polymer Composite (PAn/TiO_2) for Cathode Material in Rechargeable Battery.'' *Mater. Lett.*, **57** (9–10) 1642–1648 (2003)
15. Hou, JH, Yang, CH, Li, YF, ''Synthesis of Regioregular Side-Chain Conjugated Polythiophene and Its Application in Photovoltaic Solar Cells.'' *Synth. Met.*, **153** (1–3) 93–96 (2005)
16. Pei, J, Yu, WL, Huang, W, Heeger, AJ, ''A Novel Series of Efficient Thiophene-Based Light-Emitting Conjugated Polymers and Application in Polymer Light-Emitting Diodes.'' *Macromolecules*, **33** (7) 2462–2471 (2000)
17. Geetha, S, Rao, CRK, Vijayan, M, Trivedi, DC, ''Biosensing and Drug Delivery by Polypyrrole.'' *Anal. Chim. Acta*, **568** (1–2) 119–125 (2006)
18. Tallman, D, Spinks, G, Dominis, A, Wallace, G, ''Electroactive Conducting Polymers for Corrosion Control.'' *J. Solid State Electrochem.*, **6** (2) 73–84 (2002)
19. Mengoli, G, Munari, MT, Bianco, P, Musiani, MM, ''Anodic Synthesis of Polyaniline Coatings onto Fe Sheets.'' *J. Appl. Polym. Sci.*, **26** (12) 4247–4257 (1981)
20. Deberry, DW, ''Modification of the Electrochemical and Corrosion Behavior of Stainless-Steels with an Electroactive Coating.'' *J. Electrochem. Soc.*, **132** (5) 1022–1026 (1985)
21. Wei, Y, Wang, JG, Jia, XR, Yeh, JM, Spellane, P, ''Polyaniline as Corrosion Protection Coatings on Cold-Rolled Steel.'' *Polymer*, **36** (23) 4535–4537 (1995)
22. Ahmad, N, MacDiarmid, AG, ''Inhibition of Corrosion of Steels with the Exploitation of Conducting Polymers.'' *Synth. Met.*, **78** (2) 103–110 (1996)
23. Tallman, DE, Pae, Y, Bierwagen, GP, ''Conducting Polymers and Corrosion: Polyaniline on Steel.'' *Corrosion*, **55** (8) 779–786 (1999)
24. Rammelt, U, Nguyen, PT, Plieth, W, ''Protection of Mild Steel by Modification with Thin Films of Polymethylthiophene.'' *Electrochim. Acta*, **46** (26–27) 4251–4257 (2001)
25. Armelin, E, Pla, R, Liesa, F, Ramis, X, Iribarren, JI, Alemán, C, ''Corrosion Protection with Polyaniline and Polypyrrole as Anticorrosive Additives for Epoxy Paint.'' *Corros. Sci.*, **50** (3) 721–728 (2008)
26. Baldissera, AF, Ferreira, CA, ''Coatings Based on Electronic Conducting Polymers for Corrosion Protection of Metals.'' *Prog. Org. Coat.*, **75** (3) 241–247 (2012)

27. Guimard, NK, Gomez, N, Schmidt, CE, ''Conducting Polymers in Biomedical Engineering.'' *Prog. Polym. Sci.*, **32** (8–9) 876–921 (2007)
28. Spinks, G, Dominis, A, Wallace, G, Tallman, D, ''Electroactive Conducting Polymers for Corrosion Control.'' *J. Solid State Electrochem.*, **6** (2) 85–100 (2002)
29. Tuken, T, Yazici, B, Erbil, M, ''Polypyrrole/Polythiophene Coating for Copper Protection.'' *Prog. Org. Coat.*, **53** (1) 38–45 (2005)
30. Castagno, KRL, Dalmoro, V, Azambuja, DS, ''Characterization and Corrosion of Polypyrrole/Sodium Dodecylbenzene Sulfonate Electropolymerised on Aluminum Alloy 1100.'' *Mater. Chem. Phys.*, **130** (1–2) 721–726 (2011)
31. Sharifirad, M, Omrani, A, Rostami, AA, Khoshroo, M, ''Electrodeposition and Characterization of Polypyrrole Films on Copper.'' *J. Electroanal. Chem.*, **645** (2) 149–158 (2010)
32. Li, Y, Leung, MY, Tao, XM, Cheng, XY, Tsang, J, Yuen, CWM, ''Polypyrrole-Coated Conductive Fabrics as a Candidate for Strain Sensors.'' *J. Mater. Sci.*, **40** (15) 4093–4095 (2005)
33. Jonas, F, Schrader, L, ''Conductive Modifications of Polymers with Polypyrroles and Polythiophenes.'' *Synth. Met.*, **41** (3) 831–836 (1991)
34. Jang, JS, Lim, B, Lee, J, Hyeon, T, ''Fabrication of a Novel Polypyrrole/Poly(Methyl Methacrylate) Coaxial Nanocable Using Mesoporous Silica as a Nanoreactor.'' *Chem. Commun.*, **01** 83–84 (2001)
35. Hosseini, MG, Sabouri, M, Shahrabi, T, ''Comparison of the Corrosion Protection of Mild Steel by Polypyrrole–Phosphate and Polypyrrole–Tungstenate Coatings.'' *J. Appl. Polym. Sci.*, **110** (5) 2733–2741 (2008)
36. Khan, M, Chaudhry, AU, Hashim, S, Zahoor, MK, Iqbal, MZ, ''Recent Developments in Intrinsically Conductive Polymer Coatings for Corrosion Protection.'' *Chem. Eng. Res. Bull.*, **14** (2) 73–86 (2010)
37. Olad, A, Naseri, B, ''Preparation, Characterization and Anticorrosive Properties of a Novel Polyaniline/Clinoptilolite Nanocomposite.'' *Prog. Org. Coat.*, **67** (3) 233–238 (2010)
38. Bahrami Panah, N, Danaee, I, ''Study of the Anticorrosive Properties of Polypyrrole/Polyaniline Bilayer via Electrochemical Techniques.'' *Prog. Org. Coat.*, **68** (3) 214–218 (2010)
39. Deshpande, P, Jadhav, N, Gelling, V, Sazou, D, ''Conducting Polymers for Corrosion Protection: A Review.'' *J. Coat. Technol. Res.*, **11** (4) 473–494 (2014)
40. Qi, XN, Vetter, C, Harper, AC, Gelling, VJ, ''Electrochemical Investigations into Polypyrrole/Aluminum Flake Pigmented Coatings.'' *Prog. Org. Coat.*, **63** (3) 345–351 (2008)
41. Wicks, ZW, Jones, FN, Pappas, SP, Wicks, DA, *Organic Coatings: Science and Technology*. Wiley, Hoboken, 2007
42. Hosseini, MG, Bagheri, R, Najjar, R, ''Electropolymerization of Polypyrrole and Polypyrrole-ZnO Nanocomposites on Mild Steel and Its Corrosion Protection Performance.'' *J. Appl. Polym. Sci.*, **121** (6) 3159–3166 (2011)
43. Yan, M, Vetter, CA, Gelling, VJ, ''Electrochemical Investigations of Polypyrrole Aluminum Flake Coupling.'' *Electrochim. Acta*, **55** (20) 5576–5583 (2010)
44. Ferreira, CA, Domenech, SC, Lacaze, PC, ''Synthesis and Characterization of Polypyrrole/TiO_2 Composites on Mild Steel.'' *J. Appl. Electrochem.*, **31** (1) 49–56 (2001)
45. Lenz, DM, Delamar, M, Ferreira, CA, ''Application of Polypyrrole/TiO_2 Composite Films as Corrosion Protection of Mild Steel.'' *J. Electroanal. Chem.*, **540** 35–44 (2003)
46. Mahmoudian, MR, Basirun, WJ, Alias, Y, Ebadi, M, ''Synthesis and Characterization of Polypyrrole/Sn-Doped TiO_2 Nanocomposites (NCs) as a Protective Pigment.'' *Appl. Surf. Sci.*, **257** (20) 8317–8325 (2011)
47. Mahmoudian, MR, Basirun, WJ, Alias, Y, ''Synthesis of Polypyrrole/Ni-Doped TiO_2 Nanocomposites (NCs) as a Protective Pigment in Organic Coating.'' *Prog. Org. Coat.*, **71** (1) 56–64 (2011)
48. Rammelt, U, Duc, LM, Plieth, W, ''Improvement of Protection Performance of Polypyrrole by Dopant Anions.'' *J. Appl. Electrochem.*, **35** (12) 1225–1230 (2005)
49. He, J, Tallman, DE, Bierwagen, GP, ''Conjugated Polymers for Corrosion Control: Scanning Vibrating Electrode Studies of Polypyrrole-Aluminum Alloy Interactions.'' *J. Electrochem. Soc.*, **151** (12) B644–B651 (2004)
50. Paliwoda-Porebska, G, Rohwerder, M, Stratmann, M, Rammelt, U, Duc, L, Plieth, W, ''Release Mechanism of Electrodeposited Polypyrrole Doped with Corrosion Inhibitor Anions.'' *J. Solid State Electrochem.*, **10** (9) 730–736 (2006)
51. Sabouri, M, Shahrabi, T, Farid, HR, Hosseini, MG, ''Polypyrrole and Polypyrrole-Tungstate Electropolymerization Coatings on Carbon Steel and Evaluating Their Corrosion Protection Performance via Electrochemical Impedance Spectroscopy.'' *Prog. Org. Coat.*, **64** (4) 429–434 (2009)
52. Kamaraj, K, Karpakam, V, Sathiyanarayanan, S, Azim, SS, Venkatachari, G, ''Synthesis of Tungstate Doped Polyaniline and Its Usefulness in Corrosion Protective Coatings.'' *Electrochim. Acta*, **56** (25) 9262–9268 (2011)
53. Rohwerder, M, Michalik, A, ''Conducting Polymers for Corrosion Protection: What Makes the Difference Between Failure and Success?'' *Electrochim. Acta*, **53** (3) 1300–1313 (2007)
54. Jadhav, N, Vetter, CA, Gelling, VJ, ''The Effect of Polymer Morphology on the Performance of a Corrosion Inhibiting Polypyrrole/Aluminum Flake Composite Pigment.'' *Electrochim. Acta*, **102** 28–43 (2013)
55. Jadhav, N, Vetter, CA, Gelling, VJ, ''Characterization and Electrochemical Investigations of Polypyrrole/Aluminum Flake Composite Pigments on AA 2024-T3 Substrate.'' *ECS Trans.*, **41** (15) 75–89 (2012)
56. Jadhav, N, Gelling, VJ, ''Synthesis and Characterization of Micaceous Iron Oxide/Polypyrrole Composite Pigments and Their Application for Corrosion Protection of Cold-Rolled Steel.'' *Corrosion*, **70** (5) 464–474 (2013)
57. Warren, LF, Walker, JA, Anderson, DP, Rhodes, CG, Buckley, LJ, ''A Study of Conducting Polymer Morphology—The Effect of Dopant Anions Upon Order.'' *J. Electrochem. Soc.*, **136** (8) 2286–2295 (1989)
58. Omastova, M, Trchova, M, Kovarova, J, Stejskal, J, ''Synthesis and Structural Study of Polypyrroles Prepared in the Presence of Surfactants.'' *Synth. Met.*, **138** (3) 447–455 (2003)
59. Pigoislandureau, E, Nicolau, YF, Delamar, M, ''XPS Study of Layer-by-Layer Deposited Polypyrrole Thin-Films.'' *Synth. Met.*, **72** (2) 111–119 (1995)
60. Idla, K, Talo, A, Niemi, HEM, Forsen, O, Ylasaari, S, ''An XPS and AFM Study of Polypyrrole Coating on Mild Steel.'' *Surf. Interface Anal.*, **25** (11) 837–854 (1997)
61. Senthil, K, Yong, K, ''Growth and Characterization of Stoichiometric Tungsten Oxide Nanorods by Thermal Evaporation and Subsequent Annealing.'' *Nanotechnology*, **18** (39) 395604 (2007)
62. Golczak, S, Kanciurzewska, A, Fahlman, M, Langer, K, Langer, JJ, ''Comparative XPS Surface Study of Polyaniline Thin Films.'' *Solid State Ionics*, **179** (39) 2234–2239 (2008)
63. Kim, DY, Lee, JY, Kim, CY, Kang, ET, Tan, KL, ''Difference in Doping Behavior Between Polypyrrole Films and Powders.'' *Synth. Met.*, **72** (3) 243–248 (1995)

64. Socrates, G, *Infrared and Raman Characteristic Group Frequencies: Tables and Charts*. Wiley, Chichester, 2004
65. Shakoor, A, Rizvi, TZ, ''Synthesis and Characterization of Polypyrrole Dodecylbenzenesulfonate-Titanium Dioxide Nanocomposites.'' *J. Appl. Polym. Sci.*, **117** (2) 970–973 (2010)
66. Liang, WB, Lei, JT, Martin, CR, ''Effect of Synthesis Temperature on the Structure, Doping Level and Charge-Transport Properties of Polypyrrole.'' *Synth. Met.*, **52** (2) 227–239 (1992)
67. Kasisomayajula, SV, Qi, X, Vetter, C, Croes, K, Pavlacky, D, Gelling, VJ, ''A Structural and Morphological Comparative Study Between Chemically Synthesized and Photopolymerized Poly(pyrrole).'' *J. Coat. Technol. Res.*, **7** (2) 145–158 (2010)
68. Saravanan, C, Shekhar, RC, Palaniappan, S, ''Synthesis of Polypyrrole Using Benzoyl Peroxide as a Novel Oxidizing Agent.'' *Macromol. Chem. Phys.*, **207** (3) 342–348 (2006)
69. Turcu, R, Darabont, AL, Nan, A, Aldea, N, Macovei, D, Bica, D, Vekas, L, Pana, O, Soran, ML, Koos, AA, Biro, LP, ''New Polypyrrole-Multiwall Carbon Nanotubes Hybrid Materials.'' *J. Optoelectron. Adv. Mater.*, **8** (2) 643–647 (2006)
70. Wu, T-M, Chang, H-L, Lin, Y-W, ''Synthesis and Characterization of Conductive Polypyrrole/Multi-walled Carbon Nanotubes Composites with Improved solubility and Conductivity.'' *Compos. Sci. Technol.*, **69** (5) 639–644 (2009)
71. Li, L, Yan, G, Wu, J, Yu, X, Guo, Q, ''Preparation of Polyaniline-Metal Composite Nanospheres by In Situ Microemulsion Polymerization.'' *J. Colloid Interface Sci.*, **326** (1) 72–75 (2008)
72. Mallick, K, Witcomb, MJ, Scurrell, MS, ''Directional Assembly of Polyaniline Functionalized Gold Nanoparticles.'' *J. Phys. Condens. Matter*, **19** (19) 196225 (2007)
73. Rashid, M, Sabir, S, Rahim, AA, Waware, U, ''Polyaniline/Palm Oil Blend for Anticorrosion of Mild Steel in Saline Environment.'' *J. Appl. Chem.*, **2014** 6 (2014)
74. Ray, S, Easteal, AJ, Cooney, RP, Edmonds, NR, ''Structure and Properties of Melt-Processed PVDF/PMMA/Polyaniline Blends.'' *Mater. Chem. Phys.*, **113** (2–3) 829–838 (2009)
75. Chauhan, NPS, Ameta, R, Ameta, R, Ameta, SC, ''Thermal and Conducting Behaviour of Emeraldine Base (EB) form of Polyaniline (PANI).'' *Indian J. Chem. Technol.*, **18** (2) 118–122 (2011)
76. Zareh, EN, Moghadam, PN, Azariyan, E, Sharifian, I, ''Conductive and Biodegradable Polyaniline/Starch Blends and their Composites with Polystyrene.'' *Iran. Polym. J.*, **20** (4) 319–328 (2011)
77. Kalasad, MN, Gadyal, MA, Hiremath, RK, Ikram, IM, Mulimani, BG, Khazi, IM, Krishnan, SKA, Rabinal, MK, ''Synthesis and Characterization of Polyaniline Rubber Composites.'' *Compos. Sci. Technol.*, **68** (7–8) 1787–1793 (2008)
78. Mansfeld, F, ''Electrochemical Impedance Spectroscopy (EIS) as a New Tool for Investigating Methods of Corrosion Protection.'' *Electrochim. Acta*, **35** (10) 1533–1544 (1990)
79. Mansfeld, F, Han, LT, Lee, CC, Zhang, G, ''Evaluation of Corrosion Protection by Polymer Coatings Using Electrochemical Impedance Spectroscopy and Noise Analysis.'' *Electrochim. Acta*, **43** (19–20) 2933–2945 (1998)
80. Bonora, PL, Deflorian, F, Fedrizzi, L, ''Electrochemical Impedance Spectroscopy as a Tool for Investigating Underpaint Corrosion.'' *Electrochim. Acta*, **41** (7–8) 1073–1082 (1996)
81. Zomorodian, A, Brusciotti, F, Fernandes, A, Carmezim, MJ, Moura e Silva, T, Fernandes, JCS, Montemor, MF, ''Anticorrosion Performance of a New Silane Coating for Corrosion Protection of AZ31 Magnesium Alloy in Hank's Solution.'' *Surf. Coat. Technol.*, **206** (21) 4368–4375 (2012)
82. Muralidharan, V, ''Warburg Impedance—Basics Revisited.'' *Anti-Corros. Methods Mater.*, **44** (1) 26–29 (1997)
83. Loveday, D, Peterson, P, Rodgers, B, ''Evaluation of Organic Coatings with Electrochemical Impedance Spectroscopy—Part 2: Application of EIS to Coatings.'' *JCT CoatingsTech*, **1** (10) 88–93 (2004)
84. Krstajic, NV, Grgur, BN, Jovanovic, SM, Vojnovic, MV, ''Corrosion Protection of Mild Steel by Polypyrrole Coatings in Acid Sulfate Solutions.'' *Electrochim. Acta*, **42** (11) 1685–1691 (1997)
85. Sathiyanarayanan, S, Azim, SS, Venkatachari, G, ''A New Corrosion Protection Coating with Polyaniline-TiO_2 Composite for Steel.'' *Electrochim. Acta*, **52** (5) 2068–2074 (2007)
86. Sabouri, M, Shahrabi, T, Hosseini, MG, ''Improving Corrosion Protection Performance of Polypyrrole Coating by Tungstate Ion Dopants.'' *Russ. J. Electrochem.*, **43** (12) 1390–1397 (2007)